Emergent Materials (2024) 7:1057–1070
https://doi.org/10.1007/s42247-024-00657-6

ORIGINAL ARTICLE

Metronidazole-loaded chitosan coating for dental implants

Keerthi Atluri[1] · Jeffrey A. Banas[2] · Jaidev Chakka[3] · Gustavo Avila-Ortiz[4] · Satheesh Elangovan[4] · Aliasger K. Salem[5]

Received: 2 October 2023 / Accepted: 18 February 2024 / Published online: 5 March 2024

Abstract
Titanium and its alloys are widely used materials for biomedical devices including orthopedic/dental implants. However, peri-implantitis is associated with recurrent surgeries and remains problematic and therefore a biocompatible approach is required to reduce instances of infection. Herein, we report on the antimicrobial potential (against key oral pathogens) and biocompatibility of a novel metronidazole-loaded chitosan formulation (coating titanium surfaces) and compare the findings with those obtained for metronidazole-loaded poly-(lactide-co-glycolide) (PLGA) coatings. Titanium disc surfaces were coated with defined metronidazole-loaded polymer-based formulations and physicochemically characterized using scanning electron microscopy (SEM), Raman spectroscopy, X-ray powder diffraction (XRD), and differential scanning calorimetry (DSC). Metronidazole released at each time point was measured using high-pressure liquid chromatography (HPLC). Antimicrobial activity of the coatings was assessed using agar disk diffusion method. Biocompatibility of the coatings was evaluated using live/dead stain confocal imaging and MTS cell proliferation assay. Osseointegration was determined by measuring BMP-2 protein expression using ELISA. PLGA coatings exhibited a smooth surface morphology, whereas the chitosan coatings exhibited a rough structure. Raman spectroscopy, XRD, and DSC data indicated no evidence of physicochemical incompatibility issues of metronidazole with PLGA and high and low molecular weight chitosan. Metronidazole delivered via high ($n = 3$, $p < 0.01$) and low molecular weight chitosan ($n = 3$, $p < 0.01$) coatings had significantly enhanced antimicrobial activity against *Prevotella intermedia* (*P. intermedia*) compared to when delivered via PLGA coatings ($n = 3$). *Treponema denticola* was also tested and was found to be significantly susceptible to metronidazole loaded in low molecular weight chitosan ($n = 3$, $p < 0.05$) compared to when delivered via PLGA coatings ($n = 3$). In addition, chitosan coatings were shown to be more biocompatible and with good osseointegration potential compared to PLGA coatings as demonstrated by higher cell viability and bone morphogenic protein-2 (BMP-2) levels, respectively. A titanium implant surface coated with metronidazole that is delivered via chitosan was successfully developed and can be considered as an appealing strategy for prevention and treatment of peri-implant infection.

1 Introduction

Implants made from titanium and its alloys are used extensively in orthopedics and dentistry due to their biocompatibility, osseointegration, mechanical, and wear-resistance properties [1, 2]. Titanium-based implants have made a significant impact in these fields by enhancing the quality of life for thousands of patients. In orthopedics, be it for bone fixation, bone fusion, or joint replacement, titanium-based implants are the most widely used devices. Likewise, the introduction of titanium-based dental implants in the 1960s revolutionized the way dentistry is practiced today, aiding in the functional and esthetic rehabilitation of millions of patients around the world [3].

Osseointegration (i.e., direct structural and functional interaction between the implant surface and living bone) is

✉ Aliasger K. Salem
aliasger-salem@uiowa.edu

1 Biopharmaceutical Product & Process Development, CSL Seqirus, Holly Springs, NC, USA

2 Dental Science Building, University of Iowa, Iowa City, IA, USA

3 College of Pharmacy, The University of Texas at Austin, Austin, TX, USA

4 Department of Periodontics, University of Iowa, Iowa City, IA, USA

5 College of Pharmacy, University of Iowa, Iowa City, IA, USA

a requirement for the functional loading and long-term survival of dental implants [4]. Like periodontitis, peri-implantitis is an inflammatory disease associated with the presence of dysbiotic biofilms that affect the peri-implant tissues (i.e., mucosa and bone) and can lead to severe complications, including progressive bone loss and implant failure. Early studies employing targeted approaches highlighted the similarities in microbial profiles between periodontitis and peri-implantitis lesions, but more recent studies that utilized high throughput techniques point to a distinct profile of specific pathogens in each of these clinical entities [5]. Compared to healthy implants, an abundance of *Porphyromonas gingivalis*, *Treponema denticola*, *Tannerella forsythia*, and other specific pathogens has been observed in peri-implantitis sites. It is also well established that peri-implantitis, once initiated, typically progresses more rapidly than periodontitis due to the less robust biologic seal provided by the peri-implant mucosa [6].

A reliable therapeutic protocol to treat peri-implantitis is yet to be identified. In addition, no viable, cost-effective coatings (with potential for scale-up) that also have both antimicrobial and bone regenerative properties, including osteointegration, osteoinduction, and osteoconductive properties, have been discovered so far [7–9]. Hence, efforts should be made that contribute to the prevention of peri-implantitis as well as promote the bone regenerative properties of implants. Clinical and radiographic improvements following systemic administration of antibiotics as an adjunct to peri-implant debridement, in comparison to debridement alone [10], point to the potential for using antibiotics to not only treat but also prevent the onset of peri-implant mucositis and peri-implantitis [10]. The development of titanium implants and transmucosal abutments with an antimicrobial surface, which can be achieved using surface modification or coating, is a plausible preventive strategy [11]. Surface modification may consist of chemical covalent conjugation while coating involves physical adsorption of antimicrobials such as macromolecules, peptides, metal elements, or antibiotics on to the implant surface [11]. Furthermore, modification of the implant surfaces by coating them with various polymers including biomimetic, synthetic, natural, and micro- and nanoparticles could modify the implant surfaces making them more biocompatible adding to their bone regenerative properties [7–9, 12].

In this study, metronidazole-loaded chitosan and metronidazole-loaded PLGA coatings were compared to determine their antimicrobial potential and therefore utility as a bacteriostatic and bactericidal surface. The reason behind using PLGA as a comparison is that PLGA is a widely used polymer for most of the drug delivery purposes. PLGA is a US Food and Drug Administration (FDA)–approved biodegradable and biocompatible polymer that can be easily tailored and processed, possessing suitable physical mechanical properties and a favorable pharmacokinetic and biodistribution profile. This polymer has been researched extensively as a material component of devices designed for controlled delivery of a range of drugs for potential clinical and commercial use.

We hypothesize that chitosan may be a superior polymer to PLGA with respect to its use as a drug-loaded polymer coating dental implants due to chitosan's antibacterial and osteogenic properties. Chitosan is a natural bioactive polymer derived from microorganisms, certain fungi, as well as the exoskeletons of crustaceans and is commonly used for its antibacterial, biocompatibility and biodegradability properties [13, 14]. Chitosan is active against both gram-negative and gram-positive bacteria, fungi, and yeasts, with biocompatibility towards mammalian cells and thereby appealing for biomedical and pharmaceutical applications. Chitosan is composed of *N*-acetyl-*D*-glucosamine and *D*-glucosamine units with β binding at position 1 and 4 obtained by heterogeneous deacetylation of chitin. Chitosan is soluble in acidic solutions below its pKa ~ 6.3, at which glucosamine units (-NH2) convert into soluble protonated forms (-NH3+) [15]. Moreover, the amino group at C2 position and hydroxyl groups at C6 and C3 positions can undergo chemical derivatization resulting in improved antimicrobial, biocompatibility, and biodegradability properties [16]. Mechanisms by which chitosan exerts its antimicrobial action include but are not limited to: (i) cell wall disruption, (ii) metal chelation, and (iii) DNA complexation [17]. In the first mechanism, chitosan disrupts the cell wall by the interaction of its NH3+ amino group with the anionic phosphate groups of phospholipids present on the bacterial cell wall resulting in osmotic imbalance and peptidoglycan hydrolysis. This can eventually result in the alteration of cell membrane permeability followed by leakage of cellular content including intracellular electrolytes such as K+ ions and other components such as proteins nucleic acids and lactate dehydrogenase that subsequently results in the microbial growth inhibition [18]. In the second mechanism, amino groups of chitosan are assumed to chelate with the metal cations such as Ca^{2+} or Mg^{2+} compromising the bacterial cell wall integrity [19]. The third mechanism assumes the diffusion of chitosan hydrolysis products and their complexation with microbial DNA resulting in the inhibition of DNA replication, as well as messenger RNA (mRNA) and protein synthesis inhibition and subsequent cell death [20]. In addition to the above mechanisms, chitosan's antimicrobial properties depend on various factors such as pH, microbial type, molecular weight, degree of deacetylation, and concentration.

Both chitosan and PLGA coatings were loaded with metronidazole owing to the drug's antimicrobial properties. Metronidazole is a bactericidal nitroimidazole class drug that is bacteriostatic against facultative anaerobic bacteria such as *Porphyromonas*, *Prevotella*, *Bacteroides*,

Fusobacterium, and *Clostridium* species [21, 22]. Because metronidazole is a low molecular weight molecule, it easily diffuses across the bacterial cell membrane [23]. Following diffusion, metronidazole is reduced by the enzymatic action of pyruvate:ferredoxin oxidoreductase with its nitro group acting as an electron sink, which results in the generation of nitroso radicals [24]. The chemical reduction of metronidazole generates a concentration gradient that promotes the uptake of more drug and further promotes nitroso radical synthesis. These nitroso radicals can break microbial DNA resulting in cell lysis and death [25]. In this *in vitro* study, the synergistic antimicrobial activity of metronidazole and chitosan on titanium surfaces was explored. A coating strategy was used to develop and thoroughly characterize an antimicrobial titanium surface and evaluate its efficacy against key oral pathogens and their interaction with mesenchymal stem cells.

2 Methods

2.1 Preparation of discs

Commercially pure titanium (CpTi) discs of 1 cm^2 area and 0.05 cm thickness were polished starting from grit number 120 and then progressing to 240, 400, and 600 using a grinding paper (Buehler Carbimet special silicon carbide for metallography) fixed to a variable speed grinder-polisher (Buehler-Ecomet 3). Then, using 50 µm white aluminum oxide (Ivoclar Vivadent), the CpTi discs were sandblasted with a sandblaster (EWL Type 5423). To remove any aluminum oxide particulate remnants, the sandblasted CpTi discs were subjected to sonication in tap water for 5 min, followed by Milli-Q water for 30 min. The CpTi discs were then cleaned by soaking in methyl ethyl ketone for 15 min and acid-passivated using 30% HNO_3 for another 30 min. The discs were then rinsed for 20 min with ultrapure water and dried in a vacuum desiccator. After drying, the CpTi discs were sterilized under UV light at 300 uW/cm^2 on both sides for 10 min each.

2.2 Metronidazole disc coating

2.2.1 PLGA coating

Metronidazole (2 mg; AC210340050; Acros Organics, NJ) was dissolved in 300 µL of tetrahydrofuran (THF) (99+%, stab, with 250 ppm BHT, 30760, Alfa Aesar, Ward Hill, MA) to which 60 mg of 50:50 poly(DL-lactide-co-glycolide) (initiated with glycolic acid; inherent viscosity = 0.67 dL/g in HFIP; Durect (Pelham, AL)) was added and vortexed to ensure that the metronidazole was completely dissolved and homogeneous. The drug-polymer mixture was then uniformly pipetted by layering onto titanium disc surfaces. The discs were then transferred to Petri dishes and secured in a sterile biosafety cabinet for 24 h to ensure that the polymer coating was completely dry with no evidence of residual solvents. The polymer-coated discs were then washed three times (~5 min/wash) using 1× PBS to remove any residual solvents.

2.2.2 Chitosan coating

Metronidazole (2 mg) was dissolved in 600 µL of 2% v/v glacial acetic acid at pH 4.5 (UN2789, Fisher Chemicals, Fair Lawn, NJ) to which Super Refined PEG 300-LQ-(MH) (SR41329; CRODA; Edison, NJ) was added and vortexed to ensure complete dissolution and homogeneity of metronidazole. Chitosan (40 mg) was then added to the above mixture and vortexed until the chitosan was completely dissolved and homogeneous. In this study, two molecular weights of chitosan were used: low molecular weight (LMW) chitosan (91.1%, Brookfield viscosity — 20.00 cps (Sigma-Aldrich, St. Louis, MO)) and high molecular weight (HMW) chitosan ((deacetylated chitin, poly(D-glucosamine): 419419 (Sigma-Aldrich, St. Louis, MO) coarse ground flakes and powder)). The drug-polymer mixture was then uniformly pipetted by layering to cover the entire surface of titanium disc. The coated discs were then transferred to Petri dishes and secured in a sterile biosafety cabinet for 24 h until the polymer coating was completely dry with no evidence of residual solvents. The polymer-coated discs were then washed three times (~5 min/wash) using 1× PBS to remove any residual solvents by loading them in an incubator shaker set at 37 °C and 300 rpm.

2.3 Surface characterization

2.3.1 Scanning electron microscopy (SEM)

Morphology and surface features of the metronidazole-loaded PLGA and chitosan-coated CpTi discs were analyzed using SEM. All the samples were fixed by incubating in 4% paraformaldehyde in 0.1 M sodium cacodylate for 1 h followed by 30 min incubation in 2% (v/v) osmium tetroxide in 0.1 M sodium cacodylate. The treated samples were then sequentially dehydrated with ethanol concentration ranging from 25 to 100% (v/v) for 4 min each. Samples were then treated for 10 min with hexamethyldisilazane (HMDS) to remove any residual alcohol before mounting on aluminum stubs using carbon tape. After mounting, the samples were subjected to sputter coating with a 5-nm-thick layer of gold–palladium with an argon beam K550 sputter coater (Emitech Ltd., Kent, England) and imaged using a Hitachi S-4800 Field-Emission SEM (Hitachi Ltd., Tokyo, Japan).

Images were captured at 4 kV accelerating voltage under an argon atmosphere.

2.3.2 Confocal Raman spectroscopy

Confocal Raman spectroscopic imaging (Nicolet Almega XR Dispersive Raman; Thermo Fisher Scientific) was performed to characterize the presence of metronidazole and its interaction with PLGA and chitosan, if any. Spectra of metronidazole (control), PLGA polymer (control), LMW chitosan (control), HMW chitosan (control) and metronidazole-loaded PLGA, and the chitosan coatings were obtained with a 780-nm Ar+ laser. After auto-aligning the instrument, the excitation laser beam was focused onto the samples for spectral acquisition using an inverted optical microscope equipped with MPlan 50×/0.75 BD objective lens. Background spectrum was collected before collecting the spectrum of each sample. OMNIC for Dispersive Raman software was used to record the shifted Raman spectra (cm^{-1}) in a range of 400 to 2000 cm^{-1} at a high spectral resolution. Spectra were subjected to spatial resolution by passing the backscattered Ar+ laser image through a 100-µm slit aperture and collecting onto a thermoelectrically cooled high sensitivity silicon CCD camera (front-illuminated open electrode) with a grid size of 1024 × 256 pixels and a pixel size of 26 µm × 26 µm.

2.3.3 X-ray powder diffraction (XRD)

XRD was used to measure the degree of crystallinity and the polymorphic nature of metronidazole and the PLGA and chitosan polymers. Before subjecting the samples to XRD, the samples were homogenized into a fine powder. The samples were then analyzed using a Bruker D-5000 q-q diffractometer equipped with a Kevex energy-sensitive detector. Wide-angle X-ray scattering with coupled $2\theta/\theta$ scan type at 5−40° 2θ range and a scanning step width of 0.01° was used to measure the diffraction. Incidence and receiving slits were set at 1 mm and 0.013°, respectively. Cu radiation of 1.5418 Å at an anode voltage of 40 kV and a current of 30 mA was used to record the data and the obtained data was processed using Diffrac suite software.

2.3.4 Differential scanning calorimetry (DSC)

DSC was used to monitor the thermodynamic transitions and physical properties of metronidazole loaded in PLGA and the chitosan coatings. Approximately 10 to 15 mg of metronidazole-loaded and blank PLGA, and chitosan (LMW and HMW) sections were weighed and hermetically sealed into aluminum pans and with an empty aluminum pan acting as a reference. Samples were heated under a stream of nitrogen gas flow at a heating rate 5 °C/min from 20 to 200 °C to produce thermograms with transition temperature (Tc) and enthalpy of transition (ΔH).

2.4 Metronidazole release

2.4.1 High-pressure liquid chromatography

High-pressure liquid chromatography (HPLC; Waters 2690 Separations Module) equipped with a dual λ absorbance detector and autosampler and using a Luna C18 column (250 mm × 10 mm) with isocratic flow was used to measure the metronidazole concentration. The mobile phase comprised of 85% water and 15% acetonitrile (ACN) with 0.01% trifluoroacetic acid (TFA) and was filtered through a 0.22-µm membrane filter followed by 30 min sonication before pumping through the HPLC column. The HPLC column was prepared for the run by washing it with a methanol and water mobile phase (75:25) and equilibrating with the mobile phase mentioned earlier. After equilibration, the samples were loaded in their respective sample stations and subjected to testing with 10 µL injection volume and 315 nm detection wavelength. The mobile phase flow rate was 0.5 mL/min, and the run time was 10 min. The obtained data were collected and analyzed in Empower Pro Chromatography Manager Data Collection System (Waters). Calibration curve measurements were performed using six different concentration standards.

2.4.2 Metronidazole release study

A quantitative metronidazole release study was performed by adding metronidazole-loaded PLGA and chitosan-coated CpTi discs to wells of a 12-well cell culture plate, to which 1000 µL of 1× PBS of pH 7.4 was added. The well plates were then loaded in an incubator shaker set at 37 °C and 300 rpm. The aliquots were removed for analysis at set points of 15 min, 30 min, 1 h, 2 h, 3 h, 5 h, 7 h, 12 h, 1 day, 2 days, 3 days, 4 days, 5 days, 6 days, 7 days, 10 days, 12 days, and 15 days of incubation in 1× PBS. The collected samples were then subjected to centrifugation at 5000 g for 10 min. The supernatant was then filtered through a 0.45-µm filter to remove any particulates and analyzed using HPLC/UV.

2.5 Antimicrobial activity

2.5.1 Agar disk diffusion method

Blood agar plates (TSA w/5% sheep blood) were used for this study. Agar plates were inoculated with a standardized inoculum of the test microorganisms (*Prevotella intermedia* and *Treponema denticola*). Immediately after inoculation, titanium discs (about 6 mm in diameter), with different coatings were placed on the agar surface. Once all disks were in

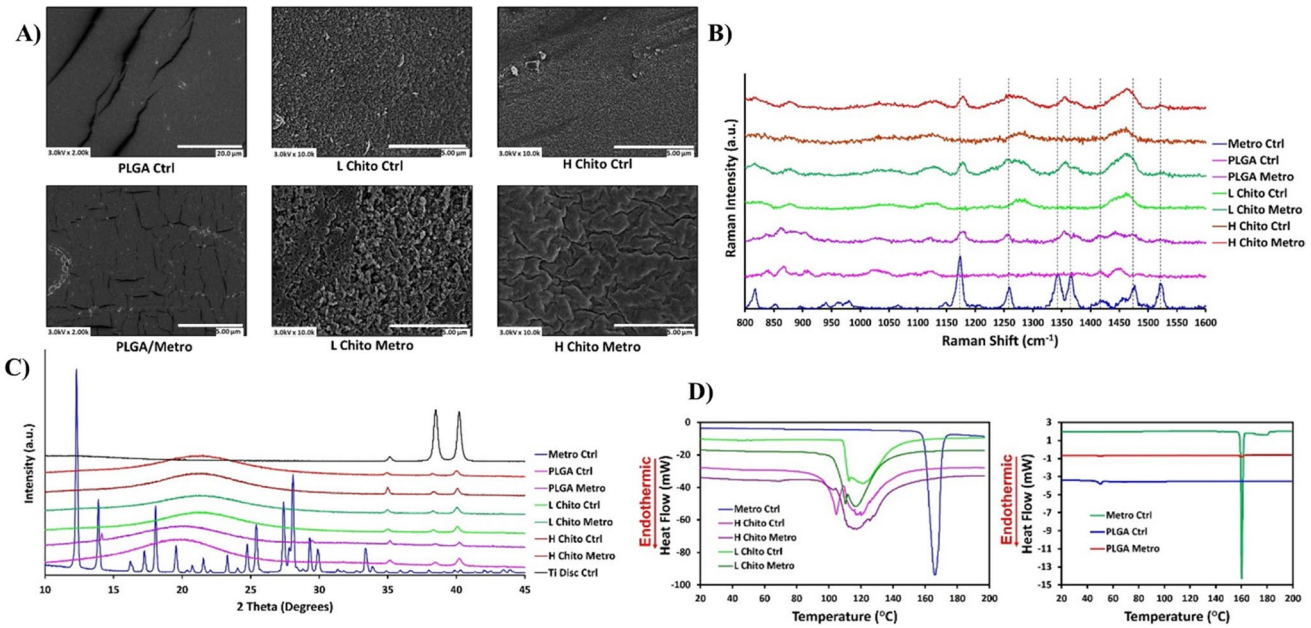

Fig. 1 **A** SEM images of CpTi discs coated with PLGA Ctrl, L Chito Ctrl, H Chito Ctrl, PLGA/Metro L Chito Metro and H Chito Metro. Size bar represents 20 µm for PLGA Ctrl and 5 µm for all other images. **B** Raman spectra analysis to determine the compatibility between metronidazole and polymer (PLGA, chitosan). **C** XRD data demonstrating the polymorphic nature of metronidazole loaded in PLGA and chitosan. Note: Legend is color coded and is in reverse horizontal order to the intensity lines. **D** DSC data demonstrating the polymorphic nature of metronidazole in PLGA and chitosan coatings

place, agar plates were incubated at 37 °C in an anaerobic environment for 24 to 48 h.

2.5.2 Measurement of inhibition zones

Post-incubation, images of the agar plates with a ruler set in place were captured, and the areas of the zones of inhibition were measured using ImageJ software. The areas were measured by setting the scale bar using the ruler present in the image. Images were processed using ImageJ (NIH, Bethesda, MD) and the areas of inhibitory zones were measured. Antimicrobial activity is represented by percent inhibition of microbial growth.

The % inhibition area was calculated using the formula :

$$\left(\frac{\text{Area of Zone of Inhibition}}{\text{Total Surface Area of Culture Dish}} \text{ x } 100\right)$$

Statistical analysis was performed using a one-way ANOVA and Tukey post hoc test with n = 3.

2.6 Biological evaluation

2.6.1 Cell culture

Induced pluripotent stem cells (iPSCs) were cultured as an adherent monolayer in 75-cm^2 polystyrene cell culture flasks (Corning Incorporated, Corning, NY). The cultures were grown in Dulbecco's modified Eagle medium (DMEM) with 10% fetal bovine serum (FBS), 1% penicillin/streptomycin, and 0.1% amphotericin B and incubated in an incubator set at 37 °C and 5% CO_2 (Sanyo Scientific, Wood Dale, IL). The medium was replenished every 2 to 3 days. Cells were passaged at 70−80% confluence, and this study was conducted using iPSCs of passage numbers 5 to 8.

2.6.2 Cell viability on CpTi discs

Live/dead stain confocal imaging Cell viability after 24 h of incubation of iPSCs was tested by incubating the coated discs cultured with iPSCs (15,000 cells/disc) for 30 min in culture media containing live cell and dead cell stain such as 1 µM calcein AM (Thermo Fisher Scientific), and 1 µM ethidium homodimer-2 (Thermo Fisher Scientific) respectively. Three discs of every treatment group were used for imaging and viability analysis purposes, with each image taken in the center of each disc with an area of 10.1 mm^2. Olympus FV1000 microscope equipped with a 4× objective lens and with 488 and 543 nm lasers to excite both calcein AM and ethidium homodimer 2, respectively, was used for confocal imaging. Z-series was produced by taking sequential images every 25 µm in depth within the area of interest. This Z-series was stacked for analysis and representation purposes.

MTS cell proliferation assay Cytotoxicity of metronidazole or blank coatings of PLGA and chitosan, cultured with iPSCs, was assessed using MTS cell growth assay reagent (Cell Titer 96 AQueous One Solution cell proliferation assay, Promega Corporation). Each disc was seeded with iPSCs at a density of 15,000 cells and was placed in flat bottom 12-well cell culture plates (Costar, Corning Inc.). The CpTi disc surfaces seeded with iPSCs were then incubated in 3 mL DMEM with 10% FBS for 24 h. After 24 h, DMEM medium was replaced with 3 mL fresh DMEM containing 100 µL MTS reagent (3-(4,5-dimethylthiazol-2-yl)-5-(3-carboxymethoxyphenyl)- 2-(4-sulfophenyl)-2H-tetrazolium). The plates were then incubated for 4 h at 37 °C and 5% CO_2. The amount of soluble formazan produced (indicator of viable cells) was spectrophotometrically measured at 490 nm using SpectraMax Plus384 (Molecular Devices, Sunnyvale, CA, USA).

The cell viability was expressed with the following equation:

$$\textbf{Cell Viability}\ (\%) = \left(\frac{\text{Absorbance intensity of iPSCs Seeded on Metronidazole Loaded Chitosan (H/L) or PLGA Coated Implants}}{\text{Absorbance intensity of iPSCs Seeded on Corresponding Chitosan (H/L) or PLGA Coated Implants}} \times 100\right)$$

Values are expressed as mean ± SEM for each treatment performed in triplicate.

2.6.3 BMP-2 protein expression

The expression of hBMP-2 protein by iPSCs incubated on the PLGA and chitosan-coated active and blank CpTi discs was determined using an hBMP-2 ELISA kit (Quantikine, R&D Systems, Minneapolis, MN) and, in comparison, to the iPSCs incubated on polystyrene of 12-well plate. Each disc was plated with cells at a density of 15,000 cells/disc, and on day 4, 500 µL of the cell supernatant (no media changes were performed over the 4 days) was collected and analyzed using ELISA. The assays were carried out in high-binding clear, polystyrene, 96-well plates (R&D systems, Minneapolis, MN, USA) and in accordance with the manufacturer's protocol. Statistical analysis was performed using paired *t*-test with p-value < 0.05.

2.7 Statistics

Statistical significance ($p < 0.05$) was evaluated using one-way and two-way analysis of variance (ANOVA) and Tukey's post hoc tests and a sample size of $n = 3$ by using GraphPad PRISM (GraphPad, San Diego, CA), a statistical and graphing software. Data are expressed as mean ± standard deviation (SD).

3 Results

3.1 Surface characterization

Surface morphological details of the PLGA- and chitosan-coated CpTi discs were observed using SEM imaging (Fig. 1A). Images show that the titanium surfaces coated with PLGA exhibited a uniform and homogeneous smooth surface morphology, whereas the discs coated with chitosan showed rough morphological features throughout the surface. HMW chitosan coating was smoother than the LMW counterpart.

Raman spectroscopy was used to characterize the chemical composition of the coated surfaces and to evaluate the interactions between the polymers (PLGA and chitosan) and metronidazole (Fig. 1B). Figure 1 B shows overlaid spectra of the metronidazole control, PLGA control, PLGA–metronidazole coating, LMW chitosan control, LMW chitosan–metronidazole coating, HMW chitosan control, and HMW chitosan–metronidazole coating. Chitosan showed a band at 1462 cm^{-1} that is attributed to a $\Delta(CH_2)$ group and a band at 1280 cm^{-1} that is due to the $\Delta(CH_2)$, $\tau(CH_2)$, Δ(HCC), Δ(HOC), and Δ(COH) group vibrations. The band at 1128 cm^{-1} can be assigned to ν(C–O–C) asymmetric stretching, while the band at 1030 cm^{-1} is attributed to ν(C–C) and ν(C–O) and the band at 870 cm^{-1} is assigned to ν (C–O–C) from the β (1–4) bond. PLGA showed bands at 1452 cm^{-1} and 1418 cm^{-1} and are due to υ(CC) aromatic ring chain vibrations. The bands between 1400 and 1470 cm^{-1} are assigned to $\delta(CH_2)$ $\delta(CH_3)$ asymmetric stretching vibrations, while the bands at 1125 cm^{-1} are due to υ(C–O–C) asymmetric stretching. The band at 1023 cm^{-1}, corresponding to υ(CC), may be due to alicyclic and aliphatic chain vibrations, while the bands at 866 cm^{-1} and 840 cm^{-1} are due to υ(C–O–C) asymmetric stretching. PEG-related bands at 1242 cm^{-1} are attributed to CH_2 twisting, 1149 cm^{-1} is due to C–O stretching and CH_2 rocking, the band at 1116 cm^{-1} is assigned to C–O–C stretching, 1060 cm^{-1} is due to C–OH stretching, and the band at 842 cm^{-1} is due to CH_2CH_2OH end group vibration. Metronidazole showed a band at 1528 cm^{-1} that is attributed to NO_2 (N–O) stretching, 1074 cm^{-1} and ~1175 cm^{-1} due to C–OH, and C–O stretching, a band at 864 cm^{-1} assigned to C–NO_2 stretching, 1476 cm^{-1} due to $\delta(CH_2)$ $\delta(CH_3)$ asymmetric and υ(CC) aromatic ring chain vibrations, a band at 1360 cm^{-1} due to υ(C–(NO_2)) end group vibration, and at 1259 cm^{-1} attributed to C–O stretching. Metronidazole-loaded PLGA and HMW and LMW Chitosan coatings showed

bands at that are attributed to the main functional groups of metronidazole such as 1175 cm^{-1}, 1259 cm^{-1} for C–O stretching, 1360 cm^{-1} due to υ(C–(NO_2)) end group vibration, and 1528 cm^{-1} attributed to NO_2 (N–O) stretching. The other minor metronidazole bands at 1074 cm^{-1} due to C–OH stretching, 864 cm^{-1} assigned to C–NO_2 stretching and 1476 cm^{-1} due to δ(CH_2) δ(CH_3) asymmetric and υ(CC) aromatic ring chain vibrations cannot be differentiated from the bands from PLGA and chitosan control bands due to interference.

The X-ray diffraction patterns (Fig. 1C) of the blank, metronidazole-loaded PLGA, and chitosan coatings on CpTi discs showed the presence of Ti element as indicated by the 2θ values at 35°, 38.5°, and 40.2°. There were no detectable differences in the peak position patterns of the uncoated CpTi discs and the PLGA and chitosan-coated CpTi discs. Metronidazole showed high-intensity peaks between 2θ values of 12° and 35°; however, these peaks were not observed in the CpTi discs coated with metronidazole-loaded chitosan. CpTi discs coated with metronidazole-loaded PLGA showed very low-intensity peaks at 2θ values between 12 and 35°.

DSC thermograms (Fig. 1D) were collected for PLGA, HMW and LMW chitosan, and metronidazole API controls along with metronidazole-loaded PLGA and chitosan coatings. Metronidazole API control showed a sharp endothermic peak at 170 °C, metronidazole-loaded, and blank HMW and LMW chitosan coatings showed a broad endothermic peak at ~120 °C and metronidazole-loaded, and blank PLGA coatings showed an endothermic peak at ~50 °C.

3.2 Metronidazole release

A fixed amount of metronidazole of 2 mg per CpTi disc was loaded into the PLGA and chitosan coatings. The release of metronidazole from the polymeric coatings was estimated by long-term immersion of the coated CpTi discs in 1× PBS solution of pH 7.4 (Fig. 2A). Approximately 50% of metronidazole was released in 48 h from PLGA coatings, indicating burst release, and 100% release was obtained within a week.

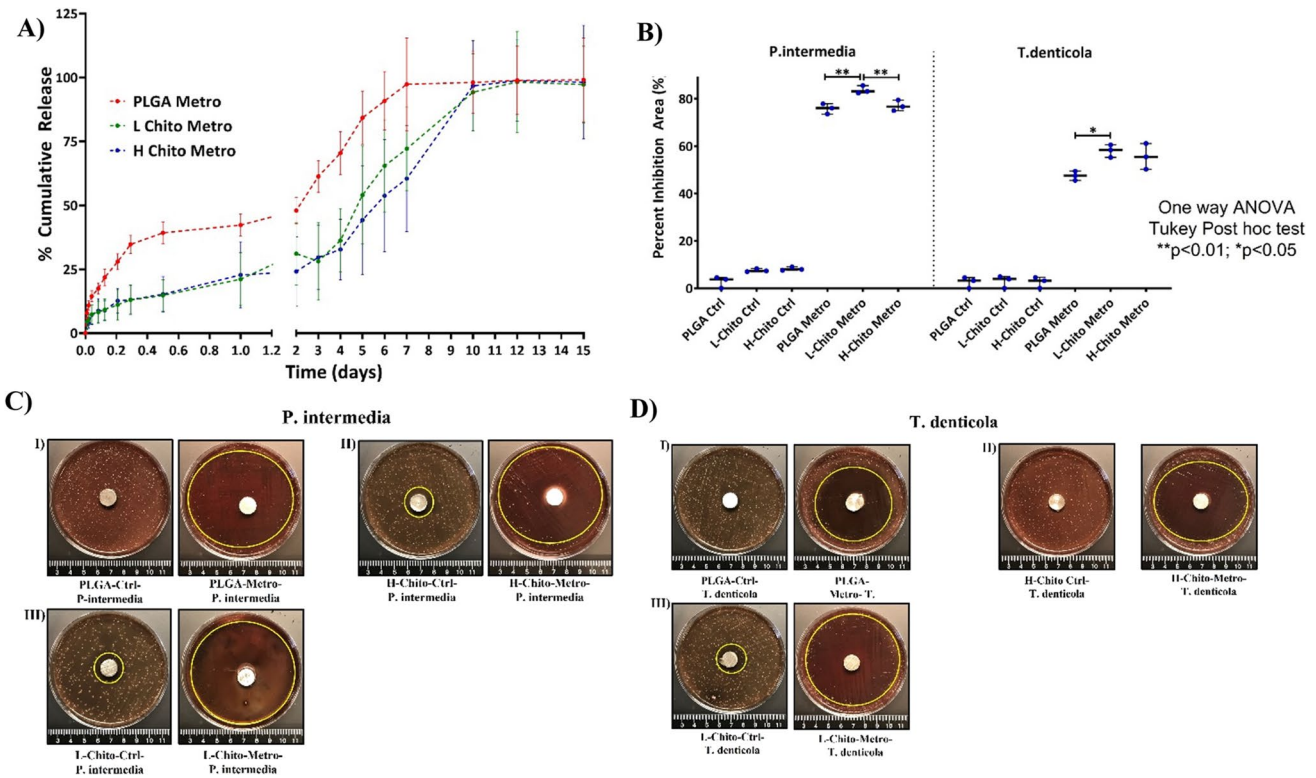

Fig. 2 **A** Determination of metronidazole release from various polymeric coatings over 15 days using HPLC analysis. **B** Graph showing percent inhibition area of Ti discs coated with PLGA Ctrl, LMW Chito Ctrl, HMW Chito Ctrl, PLGA Metro, LMW Chito Metro, HMW Chito Metro on *P. intermedia* (left) and *T. denticola* (right) coated agar plates. **C** Agar disk-diffusion method of microbial extract using *P. intermedia* as a test microorganism after 24 h of incubation of Ti discs coated with (I) PLGA Ctrl (left), PLGA Metro (right). (II) HMW Chito Ctrl (left), HMW Chito Metro (right); and (III) LMW Chito Ctrl (left), LMW Chito Metro (right). **D** Agar disk-diffusion method of microbial extract using T. denticola as a test microorganism after 24 h of incubation of CpTi discs coated with (I) PLGA Ctrl (left), PLGA Metro (right); (II) HMW Chito Ctrl (left), HMW Chito Metro (right); and (III) LMW Chito Ctrl (left), LMW Chito Metro (right)

Approximately 25% of metronidazole was released in 48 h from LMW chitosan coatings and approximately 75% release was obtained within a week and 100% release was observed at around day 10. Approximately 25% of metronidazole was released in 48 h from LMW chitosan coatings, and approximately 50% release was obtained within a week and 100% release was observed at around day 10. Metronidazole release was slower from chitosan coatings compared to PLGA coatings indicating sustained and prolonged release from chitosan. Furthermore, although the HMW chitosan released a bit slower until day 7, a similar release rate compared to LMW was obtained at day 10 indicating no significant differences in release between different molecular weights of chitosan.

3.3 Antimicrobial activity

Zones of inhibition were observed as clear distinct regions around metronidazole-loaded PLGA and chitosan-coated CpTi discs (Fig. 2B; Table 1). PLGA and HMW and LMW chitosan-coated CpTi discs showed approximately 5 to 10% inhibition of *P. intermedia* (Fig. 2C). The PLGA-coated control showed 2.75 ± 2.41%, LMW chitosan control showed 7.53 ± 0.66% and HMW chitosan control-coated control CpTi discs showed around 8.17 ± 0.74% inhibition of *P. intermedia*. In contrast, the metronidazole-loaded PLGA and metronidazole-loaded HMW and LMW chitosan-coated CpTi discs showed approximately 80 to 90% inhibition of *P. intermedia*. This result is significantly higher compared to percent inhibition areas of control groups. In addition, within the metronidazole-loaded groups, metronidazole-loaded LMW chitosan groups showed significantly higher % inhibition at 83.69 ± 1.65% compared to metronidazole-loaded HMW chitosan at 77.04 ± 2.26% ($p < 0.01$) and metronidazole-loaded PLGA at 75.82 ± 2.17% ($p < 0.01$).

PLGA-coated control and HMW/LMW chitosan-coated control CpTi discs showed around 5% inhibition of *T. denticola* (Fig. 2D). The PLGA-coated control showed 2.75 ± 2.31%, LMW chitosan control showed 2.92 ± 2.57%, and HMW chitosan-coated control CpTi discs showed around 2.59 ± 2.34% inhibition of *T. denticola*. In contrast, the metronidazole-loaded PLGA and metronidazole-loaded HMW and LMW chitosan-coated CpTi discs showed approximately 40 to 60% inhibition area for *T. denticola*. This result is significantly higher compared to percent inhibition areas of control groups. In addition, within the metronidazole-loaded groups, metronidazole-loaded LMW chitosan groups showed % area of inhibition at 58.04 ± 2.66% which is higher compared to metronidazole-loaded HMW chitosan groups at 55.6 ± 5.44% and significantly higher compared to metronidazole-loaded PLGA at 47.48 ± 1.95% ($p < 0.05$).

3.4 Biological evaluation

3.4.1 Cell viability on CpTi discs

Metronidazole-loaded PLGA and chitosan-coated CpTi discs and the corresponding blank discs cultured with iPSCs were stained with EtBr (dead stain) and calcein (live stain). Confocal images of PLGA metronidazole and PLGA control-coated CpTi discs showed comparatively higher EtBr staining and less calcein staining compared to the blank and metronidazole-loaded HMW and LMW chitosan-coated CpTi discs (qualitative comparison) (Fig. 3A). An MTS cell proliferation assay (Fig. 3B) was used to determine the cytotoxicity of the metronidazole-loaded PLGA and chitosan-coated CpTi discs using iPSCs as an in vitro cell culture model. Results show that the % cell viability of iPSCs cultured on PLGA control and PLGA metronidazole CpTi discs was 52.73 ± 17.21% and 48.93 ± 15.83%, respectively. The cell viability of iPSCs cultured on blank and metronidazole-loaded LMW chitosan-coated CpTi discs was 89.83 ± 21.31% and 81.99 ± 19.31% respectively, and the cell viability of iPSCs cultured on blank and metronidazole-loaded HMW chitosan-coated CpTi discs was 87.11 ± 21.99% and 78.09 ± 22.81%, respectively.

3.4.2 BMP-2 protein expression

BMP-2 protein expression in human iPSCs cultured on blank and metronidazole-loaded PLGA and chitosan-coated CpTi discs was measured in the supernatant using an ELISA (Fig. 3C). Results demonstrated that the human iPSCs cultured on blank and metronidazole-loaded PLGA are expressed 12.56 ± 3.2 pg/mL and 13.19 ± 1.96 pg/mL of BMP-2, respectively. The cultures on blank and metronidazole-loaded HMW chitosan expressed 23.44 ± 2.28 pg/mL and 25.94 ± 3.69 pg/mL of BMP-2, respectively. Interestingly, cultures on blank and metronidazole-loaded LMW chitosan expressed 225.31 ± 98.98 pg/mL and 182.19 ± 14.66 pg/mL of BMP-2, respectively. Though not significant, the cultures on LMW chitosan expressed higher BMP-2 levels compared to those of the BMP-2 levels expressed by iPSCs cultured on PLGA and HMW chitosan groups.

Table 1 Antimicrobial activity of indicated coatings expressed as percent inhibition

Bacteria	PLGA Ctrl	L-Chito Ctrl	H-Chito Ctrl	PLGA Metro	L-Chito Metro	H-Chito Metro
P. intermedia	2.75±2.41	7.53±0.66	8.17±0.74	75.82±2.17	83.69±1.64	77.04±2.26
T. denticola	2.57±2.31	2.92±2.57	2.59±2.34	47.48±1.95	58.07±2.61	55.60±5.44

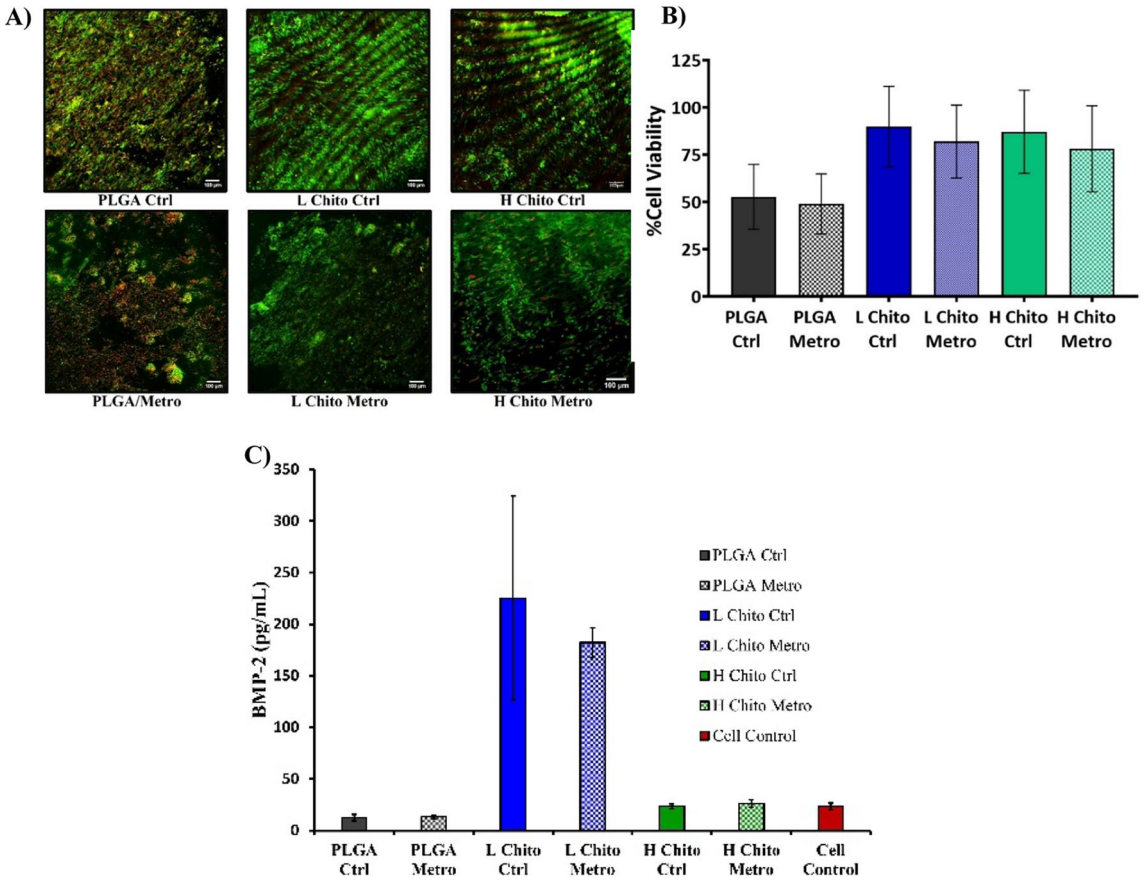

Fig. 3 **A** Live dead cell confocal images of IPSCs grown for 24 h over Ti discs coated with PLGA Ctrl, LMW Chito Ctrl, HMW Chito Ctrl, PLGA/Metro, LMW Chito Metro, and HMW Chito Metro. **B** Chart representing cell viability of the IPSCs grown for 24 h over the abovementioned coatings obtained via MTS assay. **C** Determination of BMP-2 protein expression by iPSCs cultured on various polymeric coatings and polystyrene of 12-well plate (cell control) over a 4-day period using ELISA

4 Discussion

Infections can be a potentially life-threatening or debilitating consequence of orthopedic and dental implant surgery, placing a substantial toll on the healthcare system [26]. Such infections can result from biofilms present on the surfaces of metallic implants and are traditionally treated with intravenously or orally administered antibiotics; however, systemic toxicity imposes a dosing threshold [27, 28]. Although local delivery of high concentrations of antibiotics can be achieved through powder applications, there are significant drawbacks to such an approach as outlined elsewhere [29–31]. As mentioned earlier, there is also an unmet need in dentistry to develop titanium implants that can deliver antibiotics locally from the surface in a sustained and controlled manner. In addition, upon corrosion and wear, titanium alloys also possibly release Al and V ions into the host tissue resulting in the instigation of inflammatory and immunological responses. Coatings can abrogate the dissolution of ions from the surface and makes the surface more biocompatible [32].

Thus, antimicrobial sustained release coatings are currently being explored for local delivery of antimicrobials and thereby inhibit microbial growth on the implant and transmucosal abutment surface resulting in maximum efficacy with reduced side-effects and costs. Existing coating technologies include coating with iodine and nanosilver [33, 34]. However, it is challenging to develop coatings that are non-toxic to tissues, does not affect the osseointegration, and still maintain an extended-release profile above minimum inhibitory concentration [30]. Several coatings loaded with growth factors have been tested including biomimetic coatings (e.g., ceramics), synthetic polymers (e.g., polycaprolactone, polylactide, poly(vinyl alcohol), poly(acrylic acid), and polyethylene glycol) [35, 36], natural polymers (e.g., hyaluronic acid, sodium alginate, and agarose), and micro- and nanoparticles [37, 38]. However, the abovementioned polymers have their own drawbacks when implemented to be deposited on titanium surfaces. For example, hyaluronic

acid and calcium phosphate coating require a plasma spray process during which the temperatures could exceed 500 °C and the laser structuring can reach beyond substrate boiling point 3260 °C resulting in metallurgical changes and undesired biochemical consequences [39, 40]. Other surface modification methods such as blasting, etching, and porous coatings have potential for crack initiation resulting in fatigue and reduced bending strength [39, 41]. In addition, from a manufacturing point of view, scale up can be challenging using such methods [42]. Thus, alternative coating techniques are being explored.

For example, polysaccharide coatings such as sodium alginate and agarose have excellent hydrophilicity resulting in biocompatibility and biodegradability; however, they are prone to chemical reactions in the body resulting in the loss of hydrophilicity [37, 38, 43]. Hydrophilic polymers, such as PEG and its derivatives, have non-fouling and protein resistant properties, along with their nanoparticle binding properties; however, due to their non-biodegradable nature, they tend to accumulate in lysosomes, along with suffering from oxidative damage [44, 45]. Zwitterionic polymers including phosphatidylcholine can switch between cationic, anionic, and zwitterionic properties, with their cationic nature leading to their antimicrobial properties [46]. However, the antibacterial properties of zwitterionic polymers can only be sustained for a short period of time [47]. Hydrophobic polymers such as polydimethylsiloxane exert their antimicrobial nature by reducing the surface energy of a material, thereby reducing the interaction between microbes and the material surface; however, this anti-adhesive property is short-lived [48, 49]. Given these issues, novel technologies are being explored for the development of safer and more reliable local antimicrobial delivery platforms [42, 50–54]. One strategy is to coat the implant and transmucosal abutment surfaces with polymers that have antimicrobial properties and simultaneously release antimicrobial agents by dipping or layering. One such polymer that is popularly known for its antimicrobial properties is chitosan.

Chitosan is a positively charged antibacterial polymer which, to our knowledge, has not been tested in conjunction with other antibiotics in the context of prevention and treatment of peri-implant diseases [55]. Several studies have shown that the biological activity of chitosan is independently affected by its molecular weight (MW) and degree of acetylation (DA) [56, 57]. However, the molecular weight can contribute significantly to enhancing the antimicrobial activity of chitosan compared to DA. For instance, LMW chitosan effectively reduces the growth and multiplication of several microbial species, such as *Bacillus subtilis*, *Escherichia coli*, *Staphylococcus aureus*, and *Pseudomonas aeruginosa* [58, 59]. This finding can be attributed to the size and conformation of LMW chitosan, where the mobility, attraction and ionic interaction of small chains facilitate its effective binding to the microbial membrane [58, 59]. PLGA is a proven and robust polymer as it is one of the most successfully deployed biodegradable polymers in FDA-approved and European Medicines Agency–approved medical devices [60]. PLGA-based delivery forms are well-known for providing sustained drug delivery, and by varying the monomer composition, the drug release kinetics are easily tailored [60]. However, PLGA lacks inherent antimicrobial properties. In this study, titanium discs were coated with chitosan and compared to PLGA coatings for its efficacy in exerting antimicrobial action. Furthermore, these polymer coatings were loaded with metronidazole, a widely used antimicrobial agent and a nitroimidazole-class drug that acts by damaging bacterial and protozoal DNA, leading to cell death.

There are only a few published studies that have evaluated chitosan coatings for their antimicrobial activity. For example, Yan *et al*. developed a biocomposite coating containing chitosan, silver, and hydroxyapatite via electrochemical deposition [61]. The study demonstrated that silver and chitosan can produce synergistic antimicrobial effects with 99.3% activity against *Escherichia coli* and 99.1% activity against *Staphylococcus aureus*. In another study, Zhu *et al.* showed that the surfaces of biomedical implants deposited with one-dimensional nanostructures of ZnO on chitosan-modified carbon nanotubes using atomic layer deposition demonstrated antibacterial efficacy against *Escherichia coli* and *Staphylococcus aureus* of over 73% and 98%, respectively [62]. In another study, Jennings *et al.* coated titanium implants with porous calcium phosphate microspheres mixed with chitosan via an alkyloxysilane reaction. The coating demonstrated reduced bacterial viability by up to 90% for a range of pathogens, including *Staphylococcus aureus*, *Prevotella denticola*, and *Porphyromonas gingivalis* [63]. Although all the above coatings showed efficient antimicrobial activity, none of these coatings were able to provide osteogenic activity. Furthermore, the technology used to develop these coatings is not cost-effective and difficult to scale-up.

In this study, chitosan and PLGA coatings loaded with metronidazole were fabricated successfully and compared to assess for antimicrobial efficacy along with osteogenic activity. These coatings were then characterized using SEM imaging, confocal, Raman, XRD, and DSC to understand the physicochemical compatibility of metronidazole with the polymer and solvents. Raman spectroscopy indicated no incompatibility of metronidazole with either chitosan or PLGA or the solvents used for their fabrication as demonstrated by the presence of the main peaks attributed to NO_2 (N–O) stretching, C–OH and C–O stretching, and C–NO_2 stretching. XRD data demonstrated that the metronidazole existed in amorphous form in the CpTi discs coated with metronidazole-loaded chitosan due to the absence of

high-intensity peaks between 2θ values of 12° and 35°, whereas CpTi discs coated with metronidazole-loaded PLGA showed very low-intensity peaks at 2θ values between 12 and 35°, indicating that some crystallinity is associated with metronidazole in the PLGA coatings. This discrepancy in the polymorphic behavior of metronidazole in PLGA and chitosan may be due to metronidazole being hydrophilic, resulting in its crystallization in the hydrophobic PLGA matrix but not in the hydrophilic chitosan coatings. DSC data fosters XRD results, as the sharp endothermic melting peak of metronidazole at 170 °C is absent indicating the existence of metronidazole in amorphous form in both PLGA and chitosan coatings. The amorphous nature of metronidazole can lead to its enhanced release from the polymer coatings as suggested by the release profiles. Release profiles indicated that almost 50% and 28% of the drug got released within 48 h from PLGA and chitosan coatings, respectively. Metronidazole release was slower from chitosan coatings compared to PLGA coatings indicating sustained and prolonged release from chitosan.

Antimicrobial activity was measured by assessing inhibition zones. While no significant differences in the zones of inhibition of controls were observed, chitosan controls showed a little higher percentage inhibition compared to PLGA control in *P. intermedia*. This result indicated that chitosan's antimicrobial properties might have contributed to the slight increase in the zone of inhibition compared to PLGA. The zones of inhibition of metronidazole-loaded chitosan coatings were considerably high towards both *P. intermedia* and *T. denticola* suggesting that chitosan and metronidazole may have a synergistic antimicrobial action. These results indicated that the chitosan coatings might be beneficial in exerting synergistic antimicrobial properties along with the antimicrobial drug. In addition to the antimicrobial action, biocompatibility of the agents was tested using iPSCs and live/dead stain confocal imaging. Results showed that % cell viability of iPSCs (originated from dental pulp) cultured on chitosan coatings was significantly higher compared to PLGA coatings. This result can be attributed to the hydrophilic nature of chitosan coatings compared to PLGA which is hydrophobic. The resulting hydrophilic nature of chitosan made it a better substrate suitable for cell attachment and proliferation. Thus, chitosan coatings are biocompatible and less cytotoxic compared to PLGA coatings.

In addition to biocompatibility, osteoinductivity was evaluated by measuring BMP-2 protein expression by iPSCs in the presence of polymeric coatings. Like many other proteins of the BMP family, BMP-2 is a potent molecule that can induce osteoblastic differentiation. Results indicated that BMP-2 expression was higher in chitosan coatings compared to PLGA coatings. Within chitosan, LMW chitosan exhibited higher protein expression compared to HMW chitosan coatings. These results could be attributed to the surface morphology of chitosan coatings as imaged by SEM. SEM imaging demonstrated a rough surface morphology (with higher surface area) for LMW chitosan coatings, compared to HMW chitosan and PLGA coatings that showed smooth morphology. Thus, it is apparent that the LMW chitosan coatings can be considered as an attractive choice for its antimicrobial efficacy, biocompatibility, and osteoinductive properties.

Several randomized controlled trials were performed to evaluate the effect of surface modification of titanium implants on osteogenesis including hydrophilicity, surface etching with sulfuric acid, calcium phosphate coatings, and different surface treatments [64–68]. Among all these studies, only one study, which used sulfuric acid to etch the titanium surfaces, showed increased osteogenic, osteoconductive, and osteoinductive properties [66]. One caveat of this trial is that the study did not consider researching the effect of etching on the release of ions that can elicit immunological responses over time. In addition, the antimicrobial activity of implant surfaces was not assessed. Thus, titanium surfaces coated with metronidazole-loaded chitosan, demonstrated by our group for their antimicrobial and osteogenic properties, are worth testing clinically as bone and dental implants.

5 Conclusion

In summary, a biodegradable, biocompatible metronidazole-loaded chitosan polymer coating with excellent antimicrobial and osteogenic properties has been successfully developed. Hence, the coated implants can be considered as an appealing strategy for the prevention and treatment of peri-implantitis. Future directions include *in vivo* testing in appropriate animal models that could foster the technological advancement towards clinical trial testing for possible bone and dental implant applications.

Declarations

Competing interest The authors declare that they have no conflict of interest.

References

1. L. Ottria, D. Lauritano, M. Andreasi Bassi, A. Palmieri, V. Candotto, A. Tagliabue, L. Tettamanti, Mechanical, chemical and biological aspects of titanium and titanium alloys in implant dentistry. J. Biol. Regul. Homeost. Agents. **32** (2018)
2. M. Long, H.J. Rack, Titanium alloys in total joint replacement - a materials science perspective. Biomaterials. **19** (1998). https://doi.org/10.1016/S0142-9612(97)00146-4

3. R.B. Osman, M.V. Swain, A critical review of dental implant materials with an emphasis on titanium versus zirconia. Materials. **8** (2015). https://doi.org/10.3390/ma8030932
4. K. Karthik, S. Sivakumar, V. Thangaswamy, Evaluation of implant success: a review of past and present concepts. J. Pharm. Bioallied Sci. **5** (2013). https://doi.org/10.4103/0975-7406.113310
5. G.N. Belibasakis, D. Manoil, Microbial community-driven etiopathogenesis of peri-implantitis. J. Dent. Res. **100** (2021). https://doi.org/10.1177/0022034520949851
6. D.W. Kang, S.H. Kim, Y.H. Choi, Y.K. Kim, Repeated failure of implants at the same site: a retrospective clinical study. Maxillofac. Plast. Reconstr. Surg. **41** (2019). https://doi.org/10.1186/s40902-019-0209-1
7. A.M. Inchingolo, G. Malcangi, L. Ferrante, G. Del Vecchio, F. Viapiano, A.D. Inchingolo, A. Mancini, C. Annicchiarico, F. Inchingolo, G. Dipalma, E. Minetti, A. Palermo, A. Patano, Surface coatings of dental implants: a review. J. Funct. Biomater. **14** (2023). https://doi.org/10.3390/jfb14050287
8. M.U. Joshi, S.P. Kulkarni, M. Choppadandi, M. Keerthana, G. Kapusetti, Current state of art smart coatings for orthopedic implants: a comprehensive review. Smart. Mater. Med. **4** (2023). https://doi.org/10.1016/j.smaim.2023.06.005
9. X. Chen, J. Zhou, Y. Qian, L.Z. Zhao, Antibacterial coatings on orthopedic implants. Mater. Today. Bio. **19** (2023). https://doi.org/10.1016/j.mtbio.2023.100586
10. A. Polymeri, J. van der Horst, D. Anssari Moin, D. Wismeijer, B.G. Loos, M.L. Laine, Non-surgical peri-implantitis treatment with or without systemic antibiotics: a randomized controlled clinical trial. Clin. Oral. Implants. Res. **33** (2022). https://doi.org/10.1111/clr.13914
11. H. Chouirfa, H. Bouloussa, V. Migonney, C. Falentin-Daudré, Review of titanium surface modification techniques and coatings for antibacterial applications. Acta. Biomater. **83** (2019). https://doi.org/10.1016/j.actbio.2018.10.036
12. S. Bohara, J. Suthakorn, Surface coating of orthopedic implant to enhance the osseointegration and reduction of bacterial colonization: a review. Biomater. Res. **26** (2022). https://doi.org/10.1186/s40824-022-00269-3
13. R.C.F. Cheung, T.B. Ng, J.H. Wong, W.Y. Chan, Chitosan: an update on potential biomedical and pharmaceutical applications. Mar. Drugs. **13** (2015). https://doi.org/10.3390/md13085156
14. C.P. Jiménez-Gómez, J.A. Cecilia, Chitosan: a natural biopolymer with a wide and varied range of applications. Molecules. **25** (2020). https://doi.org/10.3390/molecules25173981
15. S.I. Aiba, Studies on chitosan: 6. Relationship between N-acetyl group distribution pattern and chitinase digestibility of partially N-acetylated chitosans. Int. J. Biol. Macromol. **15** (1993)
16. D. Yu, J. Feng, H. You, S. Zhou, Y. Bai, J. He, H. Cao, Q. Che, J. Guo, Z. Su, The microstructure, antibacterial and antitumor activities of chitosan oligosaccharides and derivatives. Mar. Drugs. **20** (2022). https://doi.org/10.3390/md20010069
17. R. Teixeira-Santos, M. Lima, L.C. Gomes, F.J. Mergulhão, Antimicrobial coatings based on chitosan to prevent implant-associated infections: a systematic review. IScience. **24** (2021). https://doi.org/10.1016/j.isci.2021.103480
18. X.F. Li, X.Q. Feng, S. Yang, G.Q. Fu, T.P. Wang, Z.X. Su, Chitosan kills Escherichia coli through damage to be of cell membrane mechanism. Carbohydr. Polym. **79** (2010). https://doi.org/10.1016/j.carbpol.2009.07.011
19. Y.C. Chung, C.Y. Chen, Antibacterial characteristics and activity of acid-soluble chitosan. Bioresour. Technol. **99** (2008). https://doi.org/10.1016/j.biortech.2007.06.044
20. M. Hosseinnejad, S.M. Jafari, Evaluation of different factors affecting antimicrobial properties of chitosan. Int. J. Biol. Macromol. **85** (2016). https://doi.org/10.1016/j.ijbiomac.2016.01.022
21. S. Löfmark, C. Edlund, C.E. Nord, Metronidazole is still the drug of choice for treatment of anaerobic infections. Clin. Infect. Dis. (2010). https://doi.org/10.1086/647939
22. J.E. Rosenblatt, R.S. Edson, Symposium on antimicrobial agents. Metronidazole., Mayo Clinic Proceedings. Mayo. Clinic. **62** (1987)
23. C.R. Tjampakasari, D.S. Prasetyo, I. Ningsih, A. Kiranasari, Distribution of anaerobic bacteria and their sensitivity pattern to several antibiotics at the clinical microbiology laboratory of School of Medicine, Universitas Indonesia, Jakarta in 2019-2020. Iran. J. Microbiol. **14** (2022). https://doi.org/10.18502/ijm.v14i1.8797
24. J. Müller, P. Schildknecht, N. Müller, Metabolism of nitro drugs metronidazole and nitazoxanide in Giardia lamblia: characterization of a novel nitroreductase (GLNR2). J. Antimicrob. Chemother. **68** (2013). https://doi.org/10.1093/jac/dkt106
25. S.A. Dingsdag, N. Hunter, Metronidazole: an update on metabolism, structure-cytotoxicity and resistance mechanisms. J. Antimicrob. Chemother. **73** (2018). https://doi.org/10.1093/jac/dkx351
26. M. Ribeiro, F.J. Monteiro, M.P. Ferraz, Infection of orthopedic implants with emphasis on bacterial adhesion process and techniques used in studying bacterial-material interactions. Biomatter. **2** (2012). https://doi.org/10.4161/biom.22905
27. M. Wang, T. Tang, Surface treatment strategies to combat implant-related infection from the beginning. J. Orthop. Translat. **17** (2019). https://doi.org/10.1016/j.jot.2018.09.001
28. W. Xi, V. Hegde, S.D. Zoller, H.Y. Park, C.M. Hart, T. Kondo, C.D. Hamad, Y. Hu, A.H. Loftin, D.O. Johansen, Z. Burke, S. Clarkson, C. Ishmael, K. Hori, Z. Mamouei, H. Okawa, I. Nishimura, N.M. Bernthal, T. Segura, Point-of-care antimicrobial coating protects orthopaedic implants from bacterial challenge. Nat. Commun. **12** (2021). https://doi.org/10.1038/s41467-021-25383-z
29. W. Liawrungrueang, S. Ungphaiboon, A. Jitsurong, N. Ingviya, B. Tangtrakulwanich, V. Yuenyongviwat, In vitro elution characteristics of gentamicin-impregnated polymethylmethacrylate: premixed with a second powder vs. liquid lyophilization. BMC. Musculoskelet. Disord. **22** (2021). https://doi.org/10.1186/s12891-020-03923-w
30. V. Wall, T.H. Nguyen, N. Nguyen, P.A. Tran, Controlling antibiotic release from polymethylmethacrylate bone cement. Biomedicines. **9** (2021). https://doi.org/10.3390/BIOMEDICINES9010026
31. T.A.G. van Vugt, J.J. Arts, J.A.P. Geurts, Antibiotic-loaded polymethylmethacrylate beads and spacers in treatment of orthopedic infections and the role of biofilm formation. Front. Microbiol. **10** (2019). https://doi.org/10.3389/fmicb.2019.01626
32. E.C. Kim, M.K. Kim, R. Leesungbok, S.W. Lee, S.J. Ahn, Co–Cr dental alloys induces cytotoxicity and inflammatory responses via activation of Nrf2/antioxidant signaling pathways in human gingival fibroblasts and osteoblasts. Dent. Mater. **32** (2016). https://doi.org/10.1016/j.dental.2016.09.017
33. H. Tsuchiya, T. Shirai, H. Nishida, H. Murakami, T. Kabata, N. Yamamoto, K. Watanabe, J. Nakase, Innovative antimicrobial coating of titanium implants with iodine. J. Orthop. Sci. **17** (2012). https://doi.org/10.1007/s00776-012-0247-3
34. J. Gallo, A. Panacek, R. Prucek, E. Kriegova, S. Hradilova, M. Hobza, M. Holinka, Silver nanocoating technology in the prevention of prosthetic joint infection. Materials. **9** (2016). https://doi.org/10.3390/ma9050337
35. Z. Zhou, D.R. Calabrese, W. Taylor, J.A. Finlay, M.E. Callow, J.A. Callow, D. Fischer, E.J. Kramer, C.K. Ober, Amphiphilic triblock copolymers with PEGylated hydrocarbon structures as environmentally friendly marine antifouling and fouling-release coatings. Biofouling. **30** (2014). https://doi.org/10.1080/08927014.2014.897335
36. D. Shang, X. Sun, X. Shen, J. Hang, L. Jin, L. Shi, Effects of PEG-TMS on the stability and antifouling performances of

hydrocarbon-modified amphiphilic xerogel coatings. Prog. Org. Coat. **121** (2018). https://doi.org/10.1016/j.porgcoat.2018.04.029
37. F.S. Palumbo, A. Volpe Bavuso, M.G. Cusimano, G. Pitarresi, G. Giammona, D. Schillaci, A polycarboxylic/amino functionalized hyaluronic acid derivative for the production of pH sensible hydrogels in the prevention of bacterial adhesion on biomedical surfaces. Int. J. Pharm. **478** (2015). https://doi.org/10.1016/j.ijpharm.2014.11.015
38. D. Alves, T. Sileika, P.B. Messersmith, M.O. Pereira, Polydopamine- mediated immobilization of alginate lyase to prevent P. aeruginosa adhesion. Macromol. Biosci. (2016). https://doi.org/10.1002/mabi.201600077
39. S.R. Radin, P. Ducheyne, Plasma spraying induced changes of calcium phosphate ceramic characteristics and the effect on in vitro stability. J. Mater. Sci. Mater. Med. **3** (1992). https://doi.org/10.1007/BF00702942
40. Y. Yang, K.H. Kim, C.M. Agrawal, J.L. Ong, Interaction of hydroxyapatite-titanium at elevated temperature in vacuum environment. Biomaterials. **25** (2004). https://doi.org/10.1016/j.biomaterials.2003.09.072
41. S. Yue, R.M. Pilliar, G.C. Weatherly, The fatigue strength of porous-coated Ti–6% Al–4% V implant alloy. J. Biomed. Mater. Res. **18** (1984). https://doi.org/10.1002/jbm.820180908
42. H. Wei, X. Song, P. Liu, X. Liu, X. Yan, L. Yu, Antimicrobial coating strategy to prevent orthopaedic device-related infections: recent advances and future perspectives. Biomater. Adv. **135** (2022). https://doi.org/10.1016/j.bioadv.2022.212739
43. L. Xu, D. Pranantyo, K.G. Neoh, E.T. Kang, Tea stains-inspired antifouling coatings based on tannic acid-functionalized agarose. ACS. Sustain. Chem. Eng. **5** (2017). https://doi.org/10.1021/acssuschemeng.6b02737
44. L. Li, S. Chen, S. Jiang, Protein interactions with oligo(ethylene glycol) (OEG) self-assembled monolayers: OEG stability, surface packing density and protein adsorption. J. Biomater. Sci. Polym. Ed. **18** (2007). https://doi.org/10.1163/156856207782246795
45. E. Ostuni, R.G. Chapman, R.E. Holmlin, S. Takayama, G.M. Whitesides, A survey of structure-property relationships of surfaces that resist the adsorption of protein. Langmuir. **17** (2001). https://doi.org/10.1021/la010384m
46. K. Ishihara, Blood-compatible surfaces with phosphorylcholine-based polymers for cardiovascular medical devices. Langmuir. **35** (2019). https://doi.org/10.1021/acs.langmuir.8b01565
47. M.J. Jensen, A. Peel, R. Horne, J. Chamberlain, L. Xu, M.R. Hansen, C.A. Guymon, Antifouling and mechanical properties of photografted zwitterionic hydrogel thin-film coatings depend on the cross-link density. ACS. Biomater. Sci. Eng. **7** (2021). https://doi.org/10.1021/acsbiomaterials.1c00852
48. X. Xu, Y. Shao, W. Wang, L. Zhu, H. Liu, S. Yang, Fluorinated polyhedral oligomeric silsesquioxanes end-capped poly(ethylene oxide) giant surfactants: precise synthesis and interfacial behaviors. Polymer (Guildf). **186** (2020). https://doi.org/10.1016/j.polymer.2019.122055
49. W. Zheng, Y. Jia, W. Chen, G. Wang, X. Guo, X. Jiang, Universal coating from electrostatic self-assembly to prevent multidrug-resistant bacterial colonization on medical devices and solid surfaces. ACS. Appl. Mater. Interfaces. **9** (2017). https://doi.org/10.1021/acsami.7b05230
50. L. Zhang, Y. Yang, Y.H. Xiong, Y.Q. Zhao, Z. Xiu, H.M. Ren, K. Zhang, S. Duan, Y. Chen, F.J. Xu, Infection-responsive long-term antibacterial bone plates for open fracture therapy. Bioact. Mater. **25** (2023). https://doi.org/10.1016/j.bioactmat.2023.01.002
51. M. Yang, S. Qiu, E. Coy, S. Li, K. Załęski, Y. Zhang, H. Pan, G. Wang, NIR-responsive TiO2 biometasurfaces: toward in situ photodynamic antibacterial therapy for biomedical implants. Adv. Mater. **34** (2022). https://doi.org/10.1002/adma.202106314
52. F. Yang, Z. Zhang, Y. Li, C. Xiao, H. Zhang, W. Li, L. Zhan, G. Liang, Y. Chang, C. Ning, J. Zhai, Z. Zhou, P. Yu, In situ construction of black titanium oxide with a multilevel structure on a titanium alloy for photothermal antibacterial therapy. ACS. Biomater. Sci. Eng. **8** (2022). https://doi.org/10.1021/acsbiomaterials.2c00256
53. S. Zhang, Q. Chai, Z. Man, C. Tang, Z. Li, J. Zhang, H. Xu, X. Xu, C. Chen, Y. Liu, F. Guo, M. Abdalla, G. Yu, K. Zhao, B. Shi, W. Li, X. Jiang, Bioinspired nano-painting on orthopedic implants orchestrates periprosthetic anti-infection and osseointegration in a rat model of arthroplasty. Chem. Eng. J. **435** (2022). https://doi.org/10.1016/j.cej.2022.134848
54. F. Zhang, Q. Hu, Y. Wei, W. Meng, R. Wang, J. Liu, Y. Nie, R. Luo, Y. Wang, B. Shen, Surface modification of titanium implants by pH-responsive coating designed for self-adaptive antibacterial and promoted osseointegration. Chem. Eng. J. **435** (2022). https://doi.org/10.1016/j.cej.2022.134802
55. D. Raafat, H.G. Sahl, Chitosan and its antimicrobial potential - a critical literature survey. Microb. Biotechnol. **2** (2009). https://doi.org/10.1111/j.1751-7915.2008.00080.x
56. I. Younes, S. Sellimi, M. Rinaudo, K. Jellouli, M. Nasri, Influence of acetylation degree and molecular weight of homogeneous chitosans on antibacterial and antifungal activities. Int. J. Food. Microbiol. **185** (2014). https://doi.org/10.1016/j.ijfoodmicro.2014.04.029
57. C. Ardean, C.M. Davidescu, N.S. Nemeş, A. Negrea, M. Ciopec, N. Duteanu, P. Negrea, D. Duda-seiman, V. Musta, Factors influencing the antibacterial activity of chitosan and chitosan modified by functionalization. Int. J. Mol. Sci. **22** (2021). https://doi.org/10.3390/ijms22147449
58. H. Yilmaz Atay, Antibacterial activity of chitosan-based systems, Functional chitosan: drug delivery and biomedical applications, 457-489. 2020. https://doi.org/10.1007/978-981-15-0263-7_15.
59. D. Yan, Y. Li, Y. Liu, N. Li, X. Zhang, C. Yan, Antimicrobial properties of chitosan and chitosan derivatives in the treatment of enteric infections. Molecules. **26** (2021). https://doi.org/10.3390/molecules26237136
60. H.K. Makadia, S.J. Siegel, Poly Lactic-co-Glycolic Acid (PLGA) as biodegradable controlled drug delivery carrier. Polymers (Basel). **3** (2011). https://doi.org/10.3390/polym3031377
61. Y. Yan, X. Zhang, C. Li, Y. Huang, Q. Ding, X. Pang, Preparation and characterization of chitosan-silver/hydroxyapatite composite coatings on TiO2 nanotube for biomedical applications. Appl. Surf. Sci. **332** (2015). https://doi.org/10.1016/j.apsusc.2015.01.136
62. Y. Zhu, X. Liu, K.W.K. Yeung, P.K. Chu, S. Wu, Biofunctionalization of carbon nanotubes/chitosan hybrids on Ti implants by atom layer deposited ZnO nanostructures. Appl. Surf. Sci. **400** (2017). https://doi.org/10.1016/j.apsusc.2016.12.158
63. J.A. Jennings, D.A. Velasquez Pulgarin, D.L. Kunwar, J. Babu, S. Mishra, J. Bumgardner, Bacterial inhibition by chitosan coatings loaded with silver-decorated calcium phosphate microspheres. Thin. Solid. Films. **596**, 83–86 (2015). https://doi.org/10.1016/j.tsf.2015.08.060
64. K. Körmöczi, G. Komlós, P. Papócsi, F. Horváth, Á. Joób-Fancsaly, The early loading of different surface-modified implants: a randomized clinical trial. BMC. Oral. Health. **21** (2021). https://doi.org/10.1186/s12903-021-01498-z
65. K.A. Ko, S. Kim, S.H. Choi, J.S. Lee, Randomized controlled clinical trial on calcium phosphate coated and conventional SLA surface implants: 1-year study on survival rate and marginal bone level. Clin. Implant. Dent. Relat. Res. **21** (2019). https://doi.org/10.1111/cid.12823
66. M. Hasegawa, J. Saruta, M. Hirota, T. Taniyama, Y. Sugita, K. Kubo, M. Ishijima, T. Ikeda, H. Maeda, T. Ogawa, A newly created meso-, micro-, and nano-scale rough titanium surface

promotes bone-implant integration. Int. J. Mol. Sci. **21** (2020). https://doi.org/10.3390/ijms21030783
67. B. Gursoytrak, H. Ataoglu, Use of resonance frequency analysis to evaluate the effects of surface properties on the stability of different implants. Clin. Oral. Implants. Res. **31** (2020). https://doi.org/10.1111/clr.13560
68. A.M. Bielemann, A.J. Schuster, A.P. Possebon, A.R. Schinestsck, O.L. Chagas-Junior, F. Faot, Clinical performance of narrow-diameter implants with hydrophobic and hydrophilic surfaces with mandibular implant overdentures: 1-year results of a randomized clinical trial. Clin. Oral. Implants. Res. **33** (2022). https://doi.org/10.1111/clr.13851